Revista Mexicana de Astronomía y Astrofísica, 61, 154-164, (2025)

OPEN ACCESS https://doi.org/10.22201/ia.01851101p.2025.61.03.04

Gaseous Disks in White Dwarfs: Properties of the Current Sample

L. Saker [1], **M. Gómez** [1,2] **and L. García** [1]

[1] *Observatorio Astronómico de Córdoba, UNC, Argentina.*
[2] *CONICET, Argentina.*

Keywords: *Stars: white dwarfs, Stars: circumstellar matter, Line: profiles, Accretion, accretion disks*

Abstract

In recent years, the number of white dwarfs (WDs) known to feature infrared (IR) excesses attributed to circumstellar dust disks has grown significantly. Gaseous disks have also been detected in some WDs with dust. We obtained optical spectra with Gemini/GMOS for 13 WDs exhibiting IR excesses to search for gaseous components. No Ca II emission was detected, suggesting that the gas phase may be short-lived compared to the dusty stage. By combining our data with those from the literature, we compiled the largest sample (to date) of WDs with and without gaseous disks. We found no significant differences in stellar properties between the two groups, although disks with gas may be, on average, brighter. The detection rate of Ca II emission supports the idea that the gas phase persists for only a fraction of the total disk lifetime. A more definitive assessment will likely require dedicated searches for both gas and dust across large WD samples.

Resumen

En años recientes se ha incrementado de manera significativa el número de estrellas enanas blancas (WDs, por su sigla en inglés) conocidas que presentan excesos en el infrarrojo (IR), atribuidos a la presencia de discos de polvo circunestelares. En algunos de esos objetos también se han detectado discos gaseosos. Se obtuvieron espectros ópticos con Gemini/GMOS para trece WDs que muestran exceso infrarrojo, con el propósito de buscar componentes gaseosos. No se detectó emisión de Ca II, lo cual sugiere que la fase gaseosa podría ser transitoria y de menor duración que la etapa asociada con el polvo. Al combinar nuestros resultados con datos previamente publicados, se compiló la muestra más extensa (a la fecha) de WDs con y sin discos gaseosos. No se encontraron diferencias significativas en las propiedades estelares entre ambos grupos, aunque los discos con gas podrían ser, en promedio, más brillantes. La baja tasa de detección de emisión de Ca II respalda la hipótesis de que la fase gaseosa persiste solo durante una fracción del tiempo de vida total del disco.

Corresponding author: L. Saker *E-mail address:* leilasaker88@unc.edu.ar
Received: November 7, 2024 **Accepted:** August 8, 2025

1. Introduction

Since the first detection of infrared (IR) excesses around a white dwarf (WD; see Zuckerman & Becklin, 1987; Reach et al., 2005, 2009), the number of WDs with excesses has increased significantly, and approximately 60 WD are now known to have IR excesses. Satellites (or missions) such as Spitzer and WISE have greatly contributed to increasing this number (Hoard et al., 2013; Farihi, 2016). IR excesses are usually considered observational evidence of the existence of remnant planetary systems around WDs, known as debris disks. In addition, the most widely accepted explanation in the literature for the existence of these dusty disks is the accretion of debris caused by the tidal destruction of smaller rocky bodies that originally formed a planetary system orbiting the current WD (Jura, 2003; Gänsicke et al., 2012; Xu et al., 2014; Vanderburg et al., 2015).

The scenario outlined above is supported by the fact that all WDs with IR excesses have heavy elements, such as Ca, Mg, Si, and Fe, in their atmospheres (Zuckerman et al., 2003, 2010). The high gravity of cool WDs causes any possible heavy chemical element in the atmosphere to sink on time scales from a few days to a million years (Schatzman, 1958). This time is considerably shorter than the cooling time of these objects (10^8–10^9 years); therefore, these elements cannot be primordial (Paquette et al., 1986; Koester & Wilken, 2006; Koester, 2009), but rather they have been accreted relatively recently.

In addition to dusty disks, gaseous disks have been found around 21 WDs, all of them bearing debris disks (Gänsicke et al., 2006, 2007, 2008; Gänsicke, 2011; Farihi et al., 2012; Melis et al., 2012; Wilson et al., 2014; Melis et al., 2020; Dennihy et al., 2020; Gentile Fusillo et al., 2021). These gas disks are recognized by the detection of double-peaked emission lines in the 8600 Å CaII triplet. Such profiles unambiguously identify the presence of a Keplerian rotating gaseous disk around these stars (Horne & Marsh, 1986).

In this study, we present our search for a gas disk in a sample of 13 WDs with dusty disks. In §2, we analyze the spectra acquired with GMOS/Gemini. In §3, we combine our observed sample with

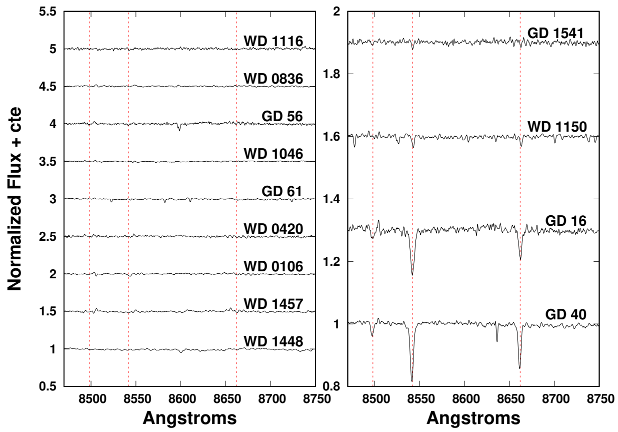

Figure 1. Gemini/GMOS spectra around de 8600 Å Ca II triplet for our observed sample (see Table 1). The normalized fluxes on the vertical scale were arbitrarily shifted to better visualize the complete sample. The dashed red lines indicate the position of the Ca II triplet.

those from the literature to derive the largest known subsample of WDs with gas disks, to compare the stellar and disk properties of WDs with and without gaseous components. Finally, in §4, we present our conclusions.

2. Observations

2.1. Target selection and data reduction

We selected a subset of 13 WDs with confirmed IR excesses; the chosen stars have temperatures between 11880-21450 K, close to the temperature range in which disks of gas have been previously detected[1]. We obtained optical spectra with the 8m Gemini telescopes using the Gemini Multi-Object Spectrograph (GMOS; Hook et al., 2004) in the longslit mode. The instrument consists of three 6266×4176 Hamamatsu CCDs, separated by two wide gaps, with a field of view (FOV) of ∼ 5.5' square.

The CCDs were binned in the spatial direction by a factor of 4, and we used the R831 grating with a central wavelength setting of 8600 Å. This setup provides a wavelength coverage of 7500-9750 Å at a resolution of 2 Å. To block 2nd-order contamination of the spectra, we used the OG515 filter. To eliminate the gaps located between the CCDs and to improve the S/N, we applied a dithering of ±50 angstroms around the central wavelength. Table 1 provides a log of our observations.

The spectra were reduced using standard spectroscopic techniques (i.e., bias subtraction, flat-fielding, wavelength calibration, sky subtraction, and finally, the extraction of the 1D spectra) using specific Gemini/GMOS IRAF routines. To perform this procedure, appropriate bias and flat-field frames were obtained from the Gemini Observatory Archive (GOA[2]). For wavelength calibration, we obtained CuAr Arcs lamps at the corresponding target elevations.

The signal-to-noise ratio (SNR) and detection limits were empirically estimated from the reduced GMOS spectra. In a line-free region of the continuum, the pixel-to-pixel noise was measured directly from the data. The noise per resolution element was then computed by multiplying the pixel noise by the square root of the full width at half-maximum (FWHM) of a representative spectral line, expressed in pixels. This yielded a value of approximately 26.4 ADU owing to the noise per resolution element.

Assuming a conservative 3σ detection threshold, the minimum detectable signal was converted into a minimum detectable equivalent width by normalizing to the continuum level and scaling by both the spectral dispersion (in Å/pixel) and the square root of the FWHM. This provides an empirical estimate of the smallest equivalent width that can be confidently detected in the spectrum. The resulting value is on the order of ∼ 0.01 Å, which defines the lower detection limit for weak absorption or emission features in the observed spectral range.

The residuals from telluric and night sky lines were carefully inspected, particularly around the Ca II triplet, and eliminated. The level of contamination from these contributions, in general, turned out to be negligible compared to the given value of the noise per resolution element.

2.2. Search of emission lines of Ca II triplet

We visually inspected the region between 8470-8750 Å of our spectra to search for the emission lines of the Ca II triplet. Figure 1 shows this region for each of the spectra. For the WDs in the left panel, the Ca II triplet appears in neither emission nor absorption. In the right panel, we show the Ca II triplet detected in absorption for GD 40 and GD 16, respectively. Klein et al. (2010) and Dennihy et al. (2017) also detected the triplet of Ca II in absorption in GD 40. WD 1150−153 and WD 1541+650 also have these lines in absorption but with lower intensity.

For WD 0420−731, WD 1046−017, WD 0836+404, and WD 1448+411, there are no previously published spectra covering the Ca II triplet region. Dennihy et al. (2017) did not find the Ca II triplet lines for WD 0110−565 and WD 0106−328. Manser et al. (2020) obtained spectra of 20 WDs with an IR excess, 9 of which are included in our sample. No WD in their sample exhibited a calcium triplet in emission.

3. Characteristics of white dwarfs with gaseous disks

In this section, we compare and analyze the properties of different WD subsamples. To obtain the stellar parameters (Table 4), we used the Montreal White Dwarf Database[3] (MWDD, Dufour et al., 2017). To ensure that the analyzed samples were as homogeneous as possible, we used the work of Vincent et al. (2024) to obtain the T_{eff} and log g values. These parameters were applied to determine the total ages of the stars using the *Wdwarfdate* open-source Python package developed by Kiman et al. (2022). *Wdwarfdate* provides main-sequence (MS), cooling, and total (MS + cooling) ages, as well as initial and final masses. The cooling ages and final masses derived from the code matched (within errors) those in the literature, confirming the consistency of our samples.

The 2MASS H (1.65 μm), K (2.17 μm) band data, WISE W1 (3.35 μm), W2 (4.60 μm) magnitudes and Gaia Data Release 2 (DR2) G_{BP} (0.513 μm), G_{RP} (0.778 μm) passbands[4] were employed to derive the color excesses in the IR, attributed to the dust disks (Table 5). The disk fractional luminosities (L_{IR}/L_*) were obtained from Rocchetto et al. (2015) and Dennihy et al. (2020). The samples are comparable because they were derived using the same methodology (Dennihy et al., 2020). In all cases, WDs with IR excesses at near-IR (Spitzer) wavelengths were selected following

[1]Caution, however, that this search as well as others (see, for example, Manser et al., 2020) did not include higher-temperature WDs because the sensitivity of detecting metallic lines in the optical declines at high temperatures (Bédard, 2024).

[2]https://archive.gemini.edu/searchform

[3]http://montrealwhitedwarfdatabase.org/.

[4]Central wavelengths of Gaia passbands are from Weiler (2018).

Table 1. Log of the Gemini/GMOS observations searching for Ca II triplet emission at WDs with a detected debris dust disk.

WD	Program	Date (UT)	Exposure (sec)	Slit (arcsec)	λ_c (Å)
WD 1448+411	GN-2016A-Q-76	2016-06-24	900	1.00	8600-8650
WD 1457−086	GN-2016A-Q-76	2016-06-25/28	900	1.00	8600-8650
WD 0106−328	GS-2016B-Q-21	2016-10-10	360	0.75	8550-8600-8650
WD 0420−731	GS-2016B-Q-21	2016-10-09/10	360	0.75	8550-8600-8650
GD 40	GS-2016B-Q-21	2016-10-09	360	0.75	8550-8600-8650
GD 61	GN-2016B-Q-56	2016-11-03	250	0.75	8550-8600-8650
WD 1046−017	GN-2017A-Q-38	2017-04-15/16	600	0.75	8550-8600-8650
WD 1150−153	GN-2017A-Q-38	2017-04-16	600	0.75	8550-8600-8650
WD 1541+650	GN-2017A-Q-38	2017-04-16	450	0.75	8550-8600-8650
GD 16	GS-2017B-Q-74	2017-08-27	400	1.00	8550-8600-8650
		2017-10-18			
GD 56	GS-2017B-Q-74	2017-08-26	450	1.00	8550-8600-8650
WD 0836+404	GN-2018A-Q-307	2018-01-20	645	1.00	8550-8600-8650
WD 1116+026	GN-2018A-Q-307	2018-01-20	600	1.00	8550-8600-8650

Table 2. Medians of the stellar parameters and color excesses related to the disk.

Parameters	Medians	
	With gas disk	Without gas disk
Mass ($M_\odot$)	0.640	0.580
T_{eff} (K)	17284	15156
log g	8	7.996
MS age (Gyr)	3.440	3.050
Cooling age (Gyr)	0.094	0.210
Total age (Gyr)	3.670	3.270
$G_{BP}-G_{RP}$	−0.235	−0.200
H−W2	1.819	1.006
W1−W2	0.532	0.477
L_{IR}/L_*	0.395	0.190

the usual criteria, using flux excesses (χ) defined as

$$\chi = \frac{F_{\rm obs} - F_{\rm model}}{\sqrt{\sigma^2_{\rm obs} + \sigma^2_{\rm model}}}, \quad (1)$$

where $F_{\rm obs}$ and $F_{\rm model}$ are the observed and model-predicted photospheric fluxes, respectively, and $\sigma_{\rm obs}$ and $\sigma_{\rm model}$ are their associated uncertainties. Significant excesses are defined as those with $\chi > 3$, which corresponds to a 3σ confidence level.

3.1. Comparison of WDs with gaseous disks with other subsamples of WDs

In order to analyze the existence of gaseous disks in WDs with dusty disks over the largest sample available to date, we combined our sample (see §2.2) with those previously reported in the literature (see for example Gänsicke et al., 2006, 2007; Manser et al., 2020; Melis et al., 2020; Wang et al., 2023). The final complete sample is presented in Appendix (Table 4). We divided the final sample into two subsamples: those with and without gas disks, depending on the detection of the Ca II triplet in emission in their spectra. It is worth mentioning that all stars in Table 4 were searched for the presence of the Ca II triplet.

We included two other subsamples in the analysis. WDs with contaminated atmospheres[5] but without IR excess and naked WDs (without/unknown contamination and IR excess). Data for these latter two groups were obtained from only two sources: Farihi et al. (2009) and Wilson et al. (2019). It is worth noting that the WDs present in both independent studies were classified into the same category –either with or without/unknown contamination or IR excess– in both studies.

Figure 2 shows W1−W2 vs cooling age (upper panel) and T_{eff} (lower panel) for four subsamples: the filled red diamonds correspond to WDs with debris and gas disks, the filled black squares to WDs with only debris disks, the empty black squares to WDs with contaminated atmospheres without IR excess, and the empty green circles represent naked WDs. WDs with uncertain 2MASS and WISE photometry were not included in these plots. We note that the four subsamples span similar ranges in cooling age and/or $T_{\rm eff}$. The only exceptions are two hot WDs with contaminated atmospheres, with $T_{\rm eff} > 60000$ K. WDs with dusty disks with and without the gas component have a large color excess (median W1−W2 = 0.53 and 0.48), suggesting that the dust component is similar in disks with and without gas. As

[5]Contaminated or Polluted WDs, in which planetary debris has contaminated otherwise pristine H or He atmospheres, are identified based on the detection of heavy metallic (magnesium, iron, calcium, etc.) lines in their spectra (Koester et al., 2014).

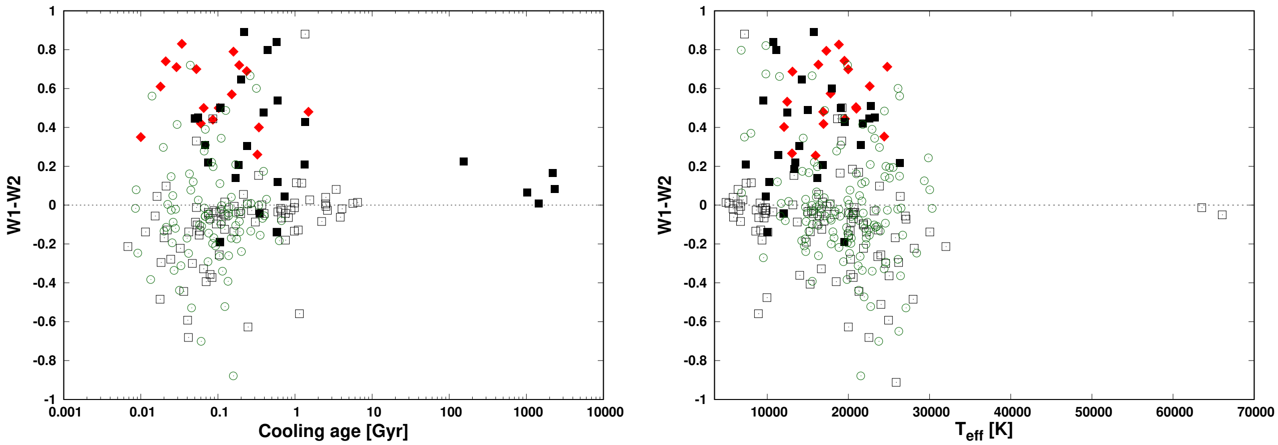

Figure 2. W1−W2 vs. age (left panel) and T_{eff} (right panel). The filled red diamonds correspond to WD with debris and gas disk, the filled black squares to WD with only debris disk, the empty black squares to WD with contaminated atmospheres without IR excess, and empty green circles represent naked WD (without/unknown contamination and IR excess).

Table 3. The Mann-Whitney U-Test applied to the analyzed subsamples.

Parameters	$p-value$
Mass	0.04036
Temperature	0.07215
log g	0.35942
MS age (Gyr)	0.23576
Cooling age (Gyr)	0.0164
Total age (Gyr)	0.27093
$G_{BP}-G_{RP}$	0.5905
H−W2	0.1795
W1−W2	0.3937
L_{IR}/L_{*}	0.11184

expected, WDs without dusty disks (with or without/unknown contaminated atmospheres) do not show a color excess (median W1−W2 = −0.137 and −0.168, respectively).

3.2. Are WDs with gaseous disks different from those with disks but without a gas component?

We compared the stellar properties of WDs with IR excesses with and without gaseous components, searching for hints that may indicate why some WDs have gas disks while others lack this component. On the other hand, we inspected the colors $G_{BP}-G_{RP}$, H−W2, W1−W2, and the fractional infrared luminosity (L_{IR}/L_{*}), as they may suggest the presence of warmer or brighter dust components in the disks. This could indicate different properties in the disks with and without gas content. Figure 3 shows the distribution of stellar parameters, whereas Figure 4 shows the distributions of the colors and fractional infrared luminosities of dusty disks with and without the gas component. The medians of all parameters analyzed are shown in Table 2.

As these histograms did not exhibit a normal distribution (i.e., a well-defined bell shape), we employed the Mann-Whitney U test (a non-parametric statistical approach) to assess the null hypothesis (H_0) that our subsamples were selected from the same parent population. This statistical test compares the ranks of randomly selected values from samples 1 and 2 and determines the probability that one sample tends to have higher values than the other. Table 3 summarizes the values obtained by applying the test. In general, the p-value represents the probability of rejecting a correct H_0, and a significance level of α =0.05 is assumed. When p< α, H_0 can be rejected with a low probability of error. Formally, the p-values of stellar parameters (mass, temperature, cooling ages, and Log g) were less than 0.05. However, we cannot claim that the samples are statistically different given the proximity of these p-values with a threshold of 0.05 chosen.

On the other hand, even though the distributions of colors and fractional infrared luminosity, L_{IR}/L_{*} are statistically similar or indistinguishable (see Table 3), the medians of infrared colors excesses (particularly in H−W2), and L_{IR}/L_{*} are significantly larger for WDs with a gas component than for WDs without gas (see Table 2). This suggests that dusty disks are brighter (or more massive) in WDs with gas than in those without a detected gas component. However, we caution that this trend is based on small samples and therefore needs to be confirmed as more observations become available.

4. Summary and conclusions

We obtained Gemini/GMOS optical spectra of 13 WDs with IR excesses to search for gaseous counterparts to dust disks based on the Ca II double-peak emission profile. No such profiles were detected in any of the WD samples.

Although the origin of the gas component in WDs' disks is not reliably known, three mechanisms have been proposed: 1) sublimation of the dust particles at the inner edge of the debris disk (Metzger et al., 2012), 2) vaporization of small solid particles originating in a collisional cascade (Kenyon & Bromley, 2017a,b), and 3) the existence of a planetesimal in a close-in orbit within the debris disk. The material in this body is sublimated by the radiation of the central WD, generating a gas component (Manser et al., 2019). In particular, these authors proposed the presence of a highly eccentric planetesimal, whose passages through the orbital periastrum would explain the variable (but periodic, P ~2h) emission found in the Ca II triplet of WD SDSS J1228+1040.

The frequency of WDs with heavy elements in their atmospheres is 25-50% (Zuckerman et al., 2003, 2010; Koester et al., 2014), and several studies have established that only 1-4% of the WDs show IR excesses (Mullally et al., 2007; Farihi et al., 2009; Barber et al., 2012; Rocchetto et al., 2015; Rebassa-Mansergas et al.,

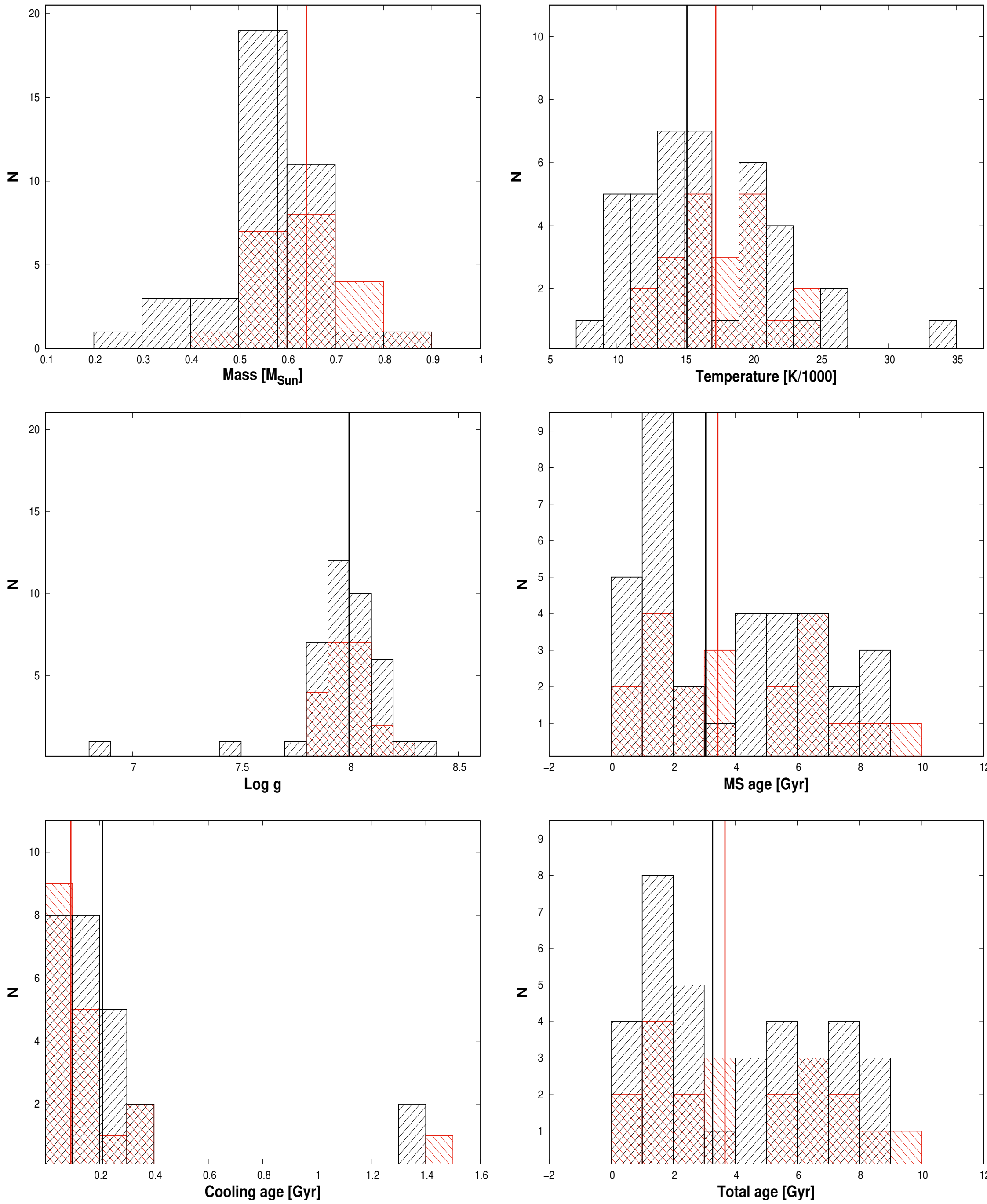

Figure 3. Histograms of the stellar parameters mass, temperature, log g, and cooling time obtained from the literature, as well as main sequence age and total age derived using *wdwarfdate*, for the analyzed subsamples: stars with (red) and without (black) disk gas detected. The red and black lines correspond to the median of each distribution.

2019; Wilson et al., 2019). Manser et al. (2020) provide the first statistical study of the frequency of gaseous components in WDs with debris disks. They estimated that only ∼4% of dusty disk WDs also show evidence of a gaseous component. Our inability to detect the Ca II triplet in the observed sample of 13 WDs is consistent with the low frequency of gaseous disks.

We combined our observed WDs with other objects from the literature to analyze the largest available sample of WDs, with and without a gaseous disk. Our results indicate that there are no significant differences in the stellar properties of WDs with and without gaseous disks. Regarding the properties of the disks, Table 4 lists the 61 WDs with confirmed dust disks for which searches for gas disks have also been carried out. Evidence of a gas disk was found in 21 of these systems (∼1/3 of the sample). This suggests that gas disks have shorter lifetimes than dust disks. Furthermore, the median L_{IR}/L_* ratio is larger for WDs with gas disks than for WDs without the gas component (Figure 4, lower right panel). This may imply that gas is predominantly present during the early

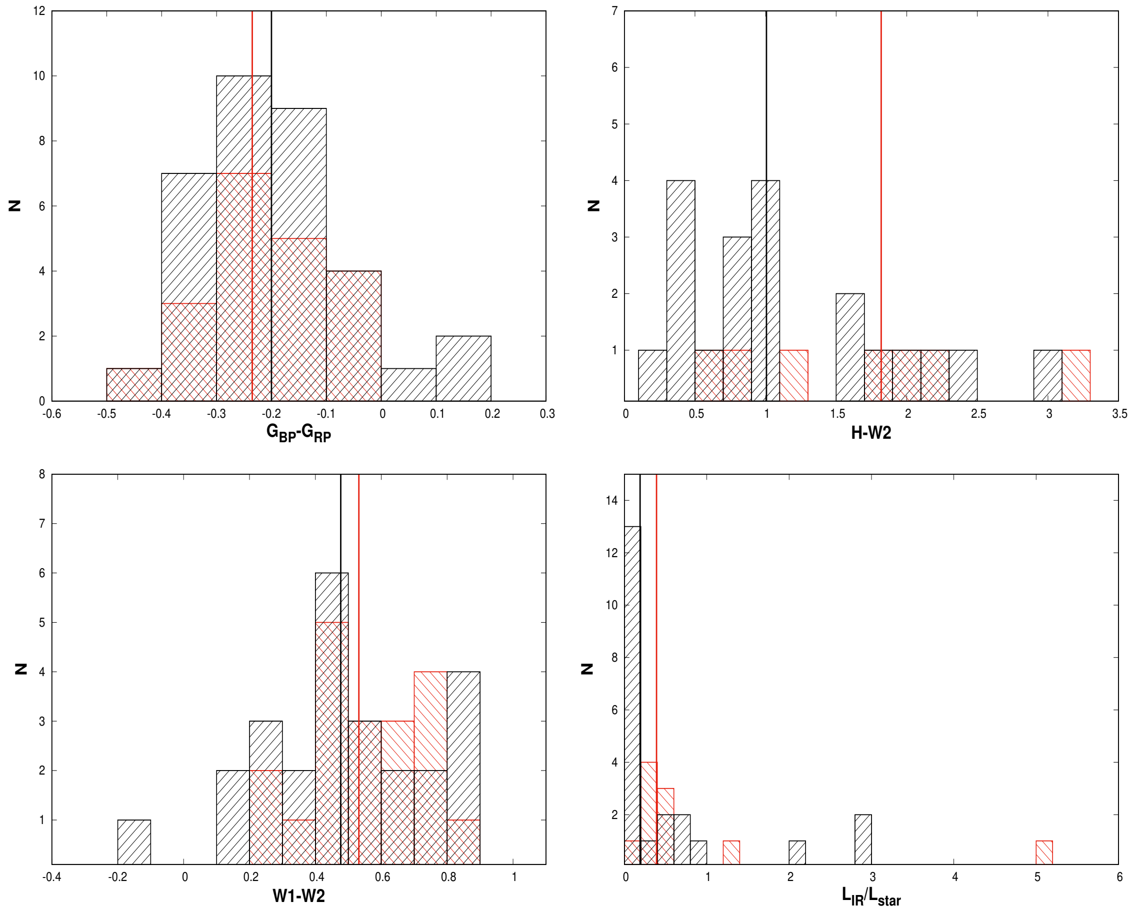

Figure 4. Histograms of color excess $G_{BP}-G_{RP}$, H$-$W2, and W1$-$W2, as well as the fractional infrared luminosity L_{IR}/L_*, for the analyzed subsamples: stars with (red) and without (black) disk gas detected. The red and black lines correspond to the median of each distribution.

stages of disk evolution and that its production decreases as the disk evolves and becomes more dynamically stable (Kenyon & Bromley, 2017b).

However, there are important caveats to consider. If the presence of a dust disk is a necessary condition for the formation of a gas disk, then estimating the gas disk fraction from a sample preselected to have dust disks may introduce a bias that favors detecting gas disks. In addition, both subsamples in Table 4 are relatively small in size. Considering these factors, the fraction of ~1/3 should be considered with caution and, at most, as an upper limit to the true occurrence rate of gas disks among dusty disk WDs. This is a different approach from that proposed by Manser et al. (2020), who estimated the frequency of gas disks using samples of WDs selected based on magnitude and/or minimum S/N requirements, regardless of the previous existence of known dust disks. From these samples, the authors derived a frequency of ~4% as mentioned above. A more definitive assessment will most likely require dedicated searches for gas and dust across large WD samples in the future.

We thank the referee for a thoughtful and thorough review of our manuscript. We are particularly grateful for the detailed comments and suggestions that improved the content and clarity of this work.

L.S. gratefully acknowledges the support from doctoral and postdoctoral fellowships from CONICET (Argentina), which made it possible to carry out most of the work presented in this paper.

Based on observations obtained at the International Gemini Observatory, a program of the NSF NOIRLab, which is managed by the Association of Universities for Research in Astronomy (AURA) under a cooperative agreement with the U.S. National Science Foundation on behalf of the Gemini Observatory partnership: The U.S. National Science Foundation (United States), National Research Council (Canada), Agencia Nacional de Investigación y Desarrollo (Chile), Ministerio de Ciencia, Tecnología e Innovación (Argentina), Ministério da Ciência, Tecnologia, Inovações e Comunicações (Brazil), and Korea Astronomy and Space Science Institute (Republic of Korea).

APPENDICES

A. Appendix

Table 4. Full sample of white dwarfs with IR excesses attributed to debris disks, ordered by T_{eff}. Stellar parameters from MWDD.

WD	T_{eff} (K)	log g	Mass ($M_\odot$)	Cooling age (Gyr)	Gas disk?	Ref.
WD 1455+298	7366	7.98	0.59	1.34	no	4, 30
WD 2115−560	9518	7.96	0.58	0.59	no	6, 36
HE 2221−1630	9824	8.11	0.67	0.73	no	4, 23
HS 0307+0746	9985	7.98	0.59	0.58	no	4, 23
WD 1225−079	10261	7.89	0.58	0.59	no	22, 29
WD 1729+371	10717	8.2	0.55	0.57	no	4, 33
WD 2326+049	11117	8	0.62	0.44	no	4, 37
WD 0836+404	11365	7.99	0.71	-	no	1, 2
WD J1221+1245	12012	8.09	0.57	0.35	no	13
SDSS J1617+1620	12073	7.98	0.61	0.34	yes	9, 11, 18
WD J0959−0200	12456	7.91	0.64	-	yes	12, 13
WD 1116+026	12503	8.06	0.64	0.39	no	1, 4, 7
SDSS J0842+2948	12771	7.71	0.44	0.24	no	42
WD 0145+234	13049	8.09	0.67	-	yes	38, 39, 40
WD J1930−5028	13104	8.02	0.55	0.24	yes	38, 39
WD 2132+096	13323	8	0.59	-	no	4, 35
WD 1554+094	13428	6.87	0.22	0.07	no	13, 24, 32
WD 1046−017	13821	8	0.58	0.24	no	1, 2
WD 1448+411	13959	7.95	0.57	0.24	no	1, 2
SDSS J1238+2910	14183	8.35	0.86	0.43	no	42
WD 2207+121	14235	7.88	0.57	0.2	no	24, 26
SDSS J0738+1835	14765	8.16	0.84	-	yes	8, 9
Gaia 2204+0233	14817	8.08	0.66	0.17	no	42
WD 1145+017	15007	8.06	-	-	no	27, 28
WD 0902+399	15089	7.46	0.33	0.09	no	42
Gaia 0155+0431	15223	7.99	0.58	0.22	no	42
WD 1551+175	15290	7.98	0.57	0.17	no	26, 31
GD 56	15744	8.07	0.59	0.22	no	1, 4, 7
SDSS J0234−0406	15949	8.25	0.71	0.32	yes	38, 39
HE 0106−3253	16156	8.04	0.62	0.17	no	1, 4, 5
WD 0842+572	16293	8	0.51	0.19	yes	38, 39, 40
GD 61	16868	8.12	0.62	0.19	no	1, 4, 6
HE 1349−2305	16891	7.97	0.67	1.49	yes	5, 17
SDSS J0347+1624	16927	7.82	0.69	0.06	yes	38, 39, 40, 41
SDSS J1043+0855	16929	8.03	0.57	0.14	yes	11, 14
Gaia J0611−6931	17284	7.95	0.74	0.16	yes	38, 39, 40, 41
Gaia J0644−0352	17800	8.04	0.72	0.15	yes	38, 39, 40, 41
WD 0420−731	17963	7.95	0.58	-	no	1, 2
WD J0529−3401	18821	7.82	0.64	0.03	yes	38, 39
WD 1015+161	19074	8.02	0.64	0.11	no	4, 7, 19
SDSS J1058+0206	19268	7.95	0.49	0.10	no	42
WD J2212−1352	19505	7.93	0.58	0.02	yes	38, 39
WD 1457−086	19515	7.88	0.38	0.11	no	1, 3, 4
WD 0110−565	19546	8.11	0.67	1.35	no	4, 5, 6
SDSS J0845+2257	19583	8.06	0.58	0.09	yes	10, 11
PG 1031+063	19736	7.86	0.51	0.07	no	42

Table 4 Stellar parameters of the full sample of white dwarfs with debris disks (cont.)

WD	T_{eff} (K)	log g	Mass ($M_{\odot}$)	Cooling age (Gyr)	Gas disk?	Ref.
SDSS J1228+1040	19970	8.04	0.73	0.05	yes	15, 16
WD 2328+107	20011	7.85	0.38	0.08	no	42
Gaia J0510+2315	20938	8.17	0.65	0.1	yes	38, 39, 40
WD 1622+587	20986	7.95	0.52	0.07	yes	38, 39, 40, 41
WD 1018+410	21520	8.07	0.57	0.07	no	13, 26
WD 0420+520	21780	8.05	0.69	-	no	4, 20
WD 0843+516	22555	7.85	0.47	0.05	no	4, 25
SDSS J0006+2858	22621	7.9	0.64	0.02	yes	38, 39, 40
EC 05365−4749	22758	8.13	0.55	-	no	4, 24
WD 1929+011	23240	8.09	0.6	0.06	no	13, 34, 35
WD J2133+2428	24408	7.84	0.57	0.01	yes	38, 39
Gaia J2100+2122	24790	8.04	0.49	0.03	yes	38, 39, 40, 41
PG 0010+281	26354	7.85	0.57	-	no	20, 21, 22
SDSS J0928+1332	26401	8.21	0.67	-	no	42
WD 1454+172	34518	8.19	0.63	0.01	no	42

References: 1) This work, 2) Hoard et al. (2013), 3) Farihi et al. (2009), 4) Manser et al. (2020), 5) Dennihy et al. (2017), 6) Girven et al. (2012), 7) Jura et al. (2007a), 8) Dufour et al. (2010), 9) Gänsicke (2011), 10) Gänsicke et al. (2008), 11) Brinkworth et al. (2012), 12) Girven et al. (2011), 13) Farihi et al. (2012), 14) Gänsicke et al. (2007), 15) Gänsicke et al. (2006), 16) Brinkworth et al. (2009), 17) Melis et al. (2012), 18) Wilson et al. (2014), 19) Gänsicke et al. (2012), 20) Barber et al. (2016), 21) Xu et al. (2015), 22) Xu et al. (2019), 23) Farihi et al. (2010), 24) Dennihy et al. (2016), 25) Xu & Jura (2012), 26) Gentile Fusillo et al. (2015), 27) Vanderburg et al. (2015), 28) Xu et al. (2016), 29) Klein et al. (2011), 30) Farihi et al. (2008), 31) Debes et al. (2019), 32) Zuckerman et al. (2003), 33) Jura et al. (2007b), 34) Vennes et al. (2010), 35) Bergfors et al. (2014), 36) Swan et al. (2019), 37) Zuckerman & Becklin (1987), 38) Gentile Fusillo et al. (2019), 39) Gentile Fusillo et al. (2021), 40) Melis et al. (2020), 41) Dennihy et al. (2020), 42) Wang et al. (2023).

Table 5. Colors and the fractional infrared luminosity L_{IR}/L_{*} of white dwarfs with debris disks (confirmed and candidates).

WD	$G_{BP}-G_{RP}$	H−W2	W1−W2	L_{IR}/L_{*}
WD 1455+298**	0.45(0.01)	0.35(0.11)	0.21(0.06)	0.19
WD 2115−560**	0.17(0.01)	0.90(0.08)	0.54(0.05)	0.84
HE 2221−1630	0.16(0.01)	0.38(0.26)	0.05(0.17)*	0.67
HS 0307+0746	0.13(0.01)	−0.23(0.45)*	−0.14(0.27)*	0.18
WD 1225−079	−0.01(0.01)*	0.19(0.14)	0.12(0.10)	0.05
WD 1729+371	0.09(0.01)	-	0.84(0.07)	2.02
WD 2326+049	0.02(0.02)*	2.33(0.05)	0.80(0.05)	2.87
WD 0836+404	0.01(0.01)*	0.33(0.23)	0.26(0.14)	-
WD J1221+1245	−0.01(0.04)*	1.93(0.37)	−0.04(0.34)*	-
SDSS J1617+1620	−0.07(0.01)	-	0.40(0.17)	1.28
WD J0959− 0100	0.08(0.08)*	1.82(0.34)	0.53(0.36)	-
WD 1116+026	−0.03(0.01)	0.97(0.09)	0.48(0.07)	0.48
SDSS J0842+2948	−0.05(003)	-	0.60(0.15)	-
WD 0145+234	−0.07(0.01)	0.70(0.09)	0.27(0.06)	-
WD J1930−5028	−0.08(0.02)	-	0.69(0.15)	-
WD 2132+096	−0.08(0.01)	−0.11(0.38)*	0.19(0.25)*	0.11
WD 1554+094	−0.29(0.05)	2.26(0.46)	0.22(0.43)*	0.43
WD 1046−017	−0.13(0.02)	-	-	-
WD 1448+411	−0.12(0.01)	-	0.30(0.13)	-
SDSS J1238+2910	−0.14(0.04)	-	0.85(0.17)	-
WD 2207+121	−0.19(0.04)	-	0.65(0.18)	0.74
SDSS J0738+1835	−0.12(0.04)	-	-	-
Gaia 2204+0233	−0.15(0.02)	-	0.15(0.41)*	-
WD 1145+017	−0.19(0.02)	1.06(0.33)	0.49(0.39)	-
WD 0902+399	−0.09(0.03)	-	-	-

Table 5 Colors and L_{IR}/L_* of white dwarfs with debris disks (cont.)

WD	$G_{BP}-G_{RP}$	H−W2	W1−W2	L_{IR}/L_*
Gaia 0155+0431	−0.12(0.02)	-	−0.14(0.11)	-
WD 1551+175	−0.18(0.02)	-	-	0.19
GD 56	−0.16(0.01)	2.98(0.16)	0.89(0.06)	2.94
SDSS J0234−0406	−0.09(0.01)	-	0.26(0.18)	-
HE 0106−3253	−0.20(0.01)	0.78(0.24)	0.14(0.11)	0.08
WD 0842+572	−0.18(0.01)	3.30(0.18)	0.72(0.05)	-
GD 61	−0.23(0.01)	0.60(0.16)	0.21(0.09)	0.28
HE 1349−2305	−0.21(0.02)	-	0.48(0.14)	0.33
SDSS J0347+1624	−0.19(0.01)	-	0.42(0.14)	0.38
SDSS J1043+0855	−0.17(0.04)	0.73(0.51)	−0.29(0.53)*	0.15
Gaia J0611−6931	−0.19(0.02)	-	0.79(0.05)	5.16
Gaia J0644−0352	−0.29(0.01)	-	0.57(0.14)	0.49
WD 0420−731	−0.24(0.01)	1.89(0.21)	0.60(0.06)	-
WD J0529−3401	−0.27(0.02)	-	0.83(0.07)	-
WD 1015+161	−0.27(0.01)	0.90(0.10)	0.50(0.12)	0.17
SDSS J1058+0206	−0.21(0.03)	0.40(0.47)*	0.52(0.59)*	-
WD J2212−1352	−0.26(0.04)	-	0.74(0.15)	-
WD 1457−086	−0.20(0.03)	0.04(0.47)*	−0.19(0.30)*	0.04
WD 0110−565	−0.29(0.01)	0.73(0.31)	0.43(0.12)	0.15
SDSS J0845+2257	−0.29(0.01)	1.24(0.15)	0.44(0.11)	0.6
PG 1031+063	−0.27(0.02)	0.41(0.29)	0.32(0.36)*	-
SDSS J1228+1040	−0.29(0.02)	1.97(0.10)	0.70(0.12)	0.4
WD 2328+107	−0.24(0.01)	0.12(0.18)*	0.22(0.24)*	0.05
Gaia J0510+2315	−0.33(0.01)	-	0.50(0.10)	-
WD 1622+587	−0.29(0.02)	-	0.50(0.09)	0.27
WD 1018+410	−0.32(0.01)	-	0.31(0.24)	0.11
WD 0420+520	−0.33(0.01)	1.54(0.22)	0.42(0.08)	-
WD 0843+516	−0.32(0.01)	1.08(0.33)	0.45(0.14)	0.13
SDSS J0006+2858	−0.34(0.02)	-	0.61(0.08)	-
EC 05365−4749	−0.35(0.01)	1.04(0.23)	0.51(0.08)	-
WD 1929+011	−0.33(0.01)	1.66(0.08)	0.45(0.06)	0.19
WD J2133+2428	−0.32(0.02)	-	0.35(0.09)	-
Gaia J2100+2122	−0.40(0.02)	2.27(0.16)	0.71(0.06)	0.39
PG 0010+281	−0.38(0.01)	0.47(0.32)	0.22(0.16)	-
SDSS J0928+1332	−0.33(0.03)	-	0.85(0.38)	-
WD 1454+172	−0.45(0.02)	-	0.74(0.28)	-

Fractional IR Luminosities, L_{IR}/L_*, were obtained from Rocchetto et al. (2015) and Dennihy et al. (2020).
* Stars discarded due to large errors in colors.
** Objects excluded because of possible contamination of nearby sources detected by visual inspection of optical and infrared images.

REFERENCES

Barber, S. D., Belardi, C., Kilic, M., & Gianninas, A. 2016, MNRAS, 459, 1415, doi: 10.1093/mnras/stw683

Barber, S. D., Patterson, A. J., Kilic, M., et al. 2012, ApJ, 760, 26, doi: 10.1088/0004-637X/760/1/26

Bédard, A. 2024, Ap&SS, 369, 43, doi: 10.1007/s10509-024-04307-5

Bergfors, C., Farihi, J., Dufour, P., & Rocchetto, M. 2014, MNRAS, 444, 2147, doi: 10.1093/mnras/stu1565

Brinkworth, C. S., Gänsicke, B. T., Girven, J. M., et al. 2012, ApJ, 750, 86, doi: 10.1088/0004-637X/750/1/86

Brinkworth, C. S., Gänsicke, B. T., Marsh, T. R., Hoard, D. W., & Tappert, C. 2009, ApJ, 696, 1402, doi: 10.1088/0004-637X/696/2/1402

Debes, J. H., Thévenot, M., Kuchner, M. J., et al. 2019, ApJ, 872, L25, doi: 10.3847/2041-8213/ab0426

Dennihy, E., Clemens, J. C., Debes, J. H., et al. 2017, ApJ, 849, 77, doi: 10.3847/1538-4357/aa8ef2

Dennihy, E., Debes, J. H., Dunlap, B. H., et al. 2016, ApJ, 831, 31, doi: 10.3847/0004-637X/831/1/31

Dennihy, E., Xu, S., Lai, S., et al. 2020, ApJ, 905, 5, doi: 10.3847/1538-4357/abc339

Dufour, P., Blouin, S., Coutu, S., et al. 2017, in ASPC, Vol. 509, 20th European White Dwarf Workshop, ed. P. E. Tremblay, B. Gaensicke, & T. Marsh, 3, doi: 10.48550/arXiv.1610.00986

Dufour, P., Kilic, M., Fontaine, G., et al. 2010, ApJ, 719, 803, doi: 10.1088/0004-637X/719/1/803

Farihi, J. 2016, NewAr, 71, 9, doi: 10.1016/j.newar.2016.03.001

Farihi, J., Gänsicke, B. T., Steele, P. R., et al. 2012, MNRAS, 421, 1635, doi: 10.1111/j.1365-2966.2012.20421.x

Farihi, J., Jura, M., Lee, J. E., & Zuckerman, B. 2010, ApJ, 714, 1386, doi: 10.1088/0004-637X/714/2/1386

Farihi, J., Jura, M., & Zuckerman, B. 2009, ApJ, 694, 805, doi: 10.1088/0004-637X/694/2/805

Farihi, J., Zuckerman, B., & Becklin, E. E. 2008, ApJ, 674, 431, doi: 10.1086/521715

Gänsicke, B. T. 2011, in AIPC, Vol. 1331, Planetary Systems Beyond the Main Sequence, ed. S. Schuh, H. Drechsel, & U. Heber (AIP), 211–214, doi: 10.1063/1.3556202

Gänsicke, B. T., Koester, D., Farihi, J., et al. 2012, MNRAS, 424, 333, doi: 10.1111/j.1365-2966.2012.21201.x

Gänsicke, B. T., Koester, D., Marsh, T. R., Rebassa-Mansergas, A., & Southworth, J. 2008, MNRAS, 391, L103, doi: 10.1111/j.1745-3933.2008.00565.x

Gänsicke, B. T., Marsh, T. R., & Southworth, J. 2007, MNRAS, 380, L35, doi: 10.1111/j.1745-3933.2007.00343.x

Gänsicke, B. T., Marsh, T. R., Southworth, J., & Rebassa-Mansergas, A. 2006, Sci, 314, 1908, doi: 10.1126/science.1135033

Gentile Fusillo, N. P., Gänsicke, B. T., & Greiss, S. 2015, MNRAS, 448, 2260, doi: 10.1093/mnras/stv120

Gentile Fusillo, N. P., Tremblay, P.-E., Gänsicke, B. T., et al. 2019, MNRAS, 482, 4570, doi: 10.1093/mnras/sty3016

Gentile Fusillo, N. P., Manser, C. J., Gänsicke, B. T., et al. 2021, MNRAS, 504, 2707, doi: 10.1093/mnras/stab992

Girven, J., Brinkworth, C. S., Farihi, J., et al. 2012, ApJ, 749, 154, doi: 10.1088/0004-637X/749/2/154

Girven, J., Gänsicke, B. T., Steeghs, D., & Koester, D. 2011, MNRAS, 417, 1210, doi: 10.1111/j.1365-2966.2011.19337.x

Hoard, D. W., Debes, J. H., Wachter, S., Leisawitz, D. T., & Cohen, M. 2013, ApJ, 770, 21, doi: 10.1088/0004-637X/770/1/21

Hook, I. M., Jørgensen, I., Allington-Smith, J. R., et al. 2004, PASP, 116, 425, doi: 10.1086/383624

Horne, K., & Marsh, T. R. 1986, MNRAS, 218, 761, doi: 10.1093/mnras/218.4.761

Jura, M. 2003, ApJ, 584, L91, doi: 10.1086/374036

Jura, M., Farihi, J., & Zuckerman, B. 2007a, ApJ, 663, 1285, doi: 10.1086/518767

Jura, M., Farihi, J., Zuckerman, B., & Becklin, E. E. 2007b, AJ, 133, 1927, doi: 10.1086/512734

Kenyon, S. J., & Bromley, B. C. 2017a, ApJ, 844, 116, doi: 10.3847/1538-4357/aa7b85

—. 2017b, ApJ, 850, 50, doi: 10.3847/1538-4357/aa9570

Kiman, R., Xu, S., Faherty, J. K., et al. 2022, AJ, 164, 62, doi: 10.3847/1538-3881/ac7788

Klein, B., Jura, M., Koester, D., & Zuckerman, B. 2011, ApJ, 741, 64, doi: 10.1088/0004-637X/741/1/64

Klein, B., Jura, M., Koester, D., Zuckerman, B., & Melis, C. 2010, ApJ, 709, 950, doi: 10.1088/0004-637X/709/2/950

Koester, D. 2009, A&A, 498, 517, doi: 10.1051/0004-6361/200811468

Koester, D., Gänsicke, B. T., & Farihi, J. 2014, A&A, 566, A34, doi: 10.1051/0004-6361/201423691

Koester, D., & Wilken, D. 2006, A&A, 453, 1051, doi: 10.1051/0004-6361:20064843

Manser, C. J., Gänsicke, B. T., Gentile Fusillo, N. P., et al. 2020, MNRAS, 493, 2127, doi: 10.1093/mnras/staa359

Manser, C. J., Gänsicke, B. T., Eggl, S., et al. 2019, Sci, 364, 66, doi: 10.1126/science.aat5330

Melis, C., Klein, B., Doyle, A. E., et al. 2020, ApJ, 905, 56, doi: 10.3847/1538-4357/abbdfa

Melis, C., Dufour, P., Farihi, J., et al. 2012, ApJ, 751, L4, doi: 10.1088/2041-8205/751/1/L4

Metzger, B. D., Rafikov, R. R., & Bochkarev, K. V. 2012, MNRAS, 423, 505, doi: 10.1111/j.1365-2966.2012.20895.x

Mullally, F., Kilic, M., Reach, W. T., et al. 2007, ApJS, 171, 206, doi: 10.1086/511858

Paquette, C., Pelletier, C., Fontaine, G., & Michaud, G. 1986, ApJS, 61, 197, doi: 10.1086/191112

Reach, W. T., Kuchner, M. J., von Hippel, T., et al. 2005, ApJ, 635, L161, doi: 10.1086/499561

Reach, W. T., Lisse, C., von Hippel, T., & Mullally, F. 2009, ApJ, 693, 697, doi: 10.1088/0004-637X/693/1/697

Rebassa-Mansergas, A., Solano, E., Xu, S., et al. 2019, MNRAS, 489, 3990, doi: 10.1093/mnras/stz2423

Rocchetto, M., Farihi, J., Gänsicke, B. T., & Bergfors, C. 2015, MNRAS, 449, 574, doi: 10.1093/mnras/stv282

Schatzman, E. L. 1958, White Dwarfs. Amsterdam, North-Holland Pub. Co.; New York, Interscience Publisher

Swan, A., Farihi, J., Koester, D., et al. 2019, MNRAS, 490, 202, doi: 10.1093/mnras/stz2337

Vanderburg, A., Johnson, J. A., Rappaport, S., et al. 2015, Natur, 526, 546, doi: 10.1038/nature15527

Vennes, S., Kawka, A., & Németh, P. 2010, MNRAS, 404, L40, doi: 10.1111/j.1745-3933.2010.00830.x

Vincent, O., Barstow, M. A., Jordan, S., et al. 2024, A&A, 682, A5, doi: 10.1051/0004-6361/202347694

Wang, L., Zhang, X., Wang, J., et al. 2023, ApJ, 944, 23, doi: 10.3847/1538-4357/acaf5a

Weiler, M. 2018, A&A, 617, A138, doi: 10.1051/0004-6361/201833462

Wilson, D. J., Gänsicke, B. T., Koester, D., et al. 2014, MNRAS, 445, 1878, doi: 10.1093/mnras/stu1876

Wilson, T. G., Farihi, J., Gänsicke, B. T., & Swan, A. 2019, MNRAS, 487, 133, doi: 10.1093/mnras/stz1050
Xu, S., Dufour, P., Klein, B., et al. 2019, AJ, 158, 242, doi: 10.3847/1538-3881/ab4cee
Xu, S., & Jura, M. 2012, ApJ, 745, 88, doi: 10.1088/0004-637X/745/1/88
Xu, S., Jura, M., Dufour, P., & Zuckerman, B. 2016, ApJ, 816, L22, doi: 10.3847/2041-8205/816/2/L22
Xu, S., Jura, M., Koester, D., Klein, B., & Zuckerman, B. 2014, ApJ, 783, 79, doi: 10.1088/0004-637X/783/2/79
Xu, S., Jura, M., Pantoja, B., et al. 2015, ApJ, 806, L5, doi: 10.1088/2041-8205/806/1/L5
Zuckerman, B., & Becklin, E. E. 1987, Natur, 330, 138, doi: 10.1038/330138a0
Zuckerman, B., Koester, D., Reid, I. N., & Hünsch, M. 2003, ApJ, 596, 477, doi: 10.1086/377492
Zuckerman, B., Melis, C., Klein, B., Koester, D., & Jura, M. 2010, ApJ, 722, 725, doi: 10.1088/0004-637X/722/1/725